



Delft University of Technology

Surface Modification of Steel Slag Aggregate for Engineering Application in Asphalt Mixture

Niu, Dongyu; Zhang, Zhao; Meng, Jiandang ; Yang, Zhengxian; Jing, Ruxin ; Liu, Xueyan; Lin, Peng; Sheng , Yanping

DOI

[10.3390/buildings13010016](https://doi.org/10.3390/buildings13010016)

Publication date

2022

Document Version

Final published version

Published in

Buildings

Citation (APA)

Niu, D., Zhang, Z., Meng, J., Yang, Z., Jing, R., Liu, X., Lin, P., & Sheng , Y. (2022). Surface Modification of Steel Slag Aggregate for Engineering Application in Asphalt Mixture. *Buildings*, 13(1), 1-20. Article 16. <https://doi.org/10.3390/buildings13010016>

Important note

To cite this publication, please use the final published version (if applicable).
Please check the document version above.

Copyright




Other than for strictly personal use, it is not permitted to download, forward or distribute the text or part of it, without the consent of the author(s) and/or copyright holder(s), unless the work is under an open content license such as Creative Commons.

Takedown policy

Please contact us and provide details if you believe this document breaches copyrights.
We will remove access to the work immediately and investigate your claim.

Article

Surface Modification of Steel Slag Aggregate for Engineering Application in Asphalt Mixture

Dongyu Niu ^{1,2}, Zhao Zhang ^{1,2}, Jiandang Meng ³, Zhengxian Yang ^{4,*} , Ruxin Jing ^{5,*} , Xueyan Liu ⁵, Peng Lin ⁵  and Yanping Sheng ^{1,2}

¹ Engineering Research Center of Transportation Materials of the Ministry of Education, Chang'an University, Xi'an 710061, China

² School of Materials Science and Engineering, Chang'an University, Xi'an 710061, China

³ Puyang Branch Office of Henan Transport Development Group Co., Ltd., Puyang 450000, China

⁴ College of Civil Engineering, Fujian Provincial University Research Center for Advanced Civil Engineering Materials, Fuzhou University, Fuzhou 350108, China

⁵ Section of Pavement Engineering, Department of Engineering Structures, Faculty of Civil Engineering and Geosciences, Delft University of Technology, Stevinweg 1, 2628 CN Delft, The Netherlands

* Correspondence: zxyang@fzu.edu.cn (Z.Y.); r.jing@tudelft.nl (R.J.)

Abstract: The proper disposal of steel slag has always been a great challenge for the metallurgical industry in China and around the world. In this work, the steel slag aggregate (SSA) was surface pretreated (PSSA) and applied into asphalt mixture. The adhesive behavior between the bitumen and five different types of aggregates (i.e., limestone, diorite, diabase, SSA, PSSA) were evaluated based on the contact angle and binder bond strength tests. The pavement performance of three asphalt mixtures which contain normal aggregate, SSA and PSSA respectively, was analyzed by Marshall stability test, wheel-tracking rutting test, low-temperature bending creep test and water sensitivity test. The results showed that surface modification can improve the surface properties of SSA, reduce its contact angle with bitumen, and eventually lead to the improvement of adhesion between them. In addition to the satisfied low-temperature properties, PSSA was found to significantly improve the anti-rutting property and reduce the water sensitivity of asphalt mixture. This work is expected to promote an alternative application for recycling of SSA in pavement engineering.

Keywords: pretreated steel slag aggregate; asphalt mixture; performance characterization; adhesion; surface energy



Citation: Niu, D.; Zhang, Z.; Meng, J.; Yang, Z.; Jing, R.; Liu, X.; Lin, P.; Sheng, Y. Surface Modification of Steel Slag Aggregate for Engineering Application in Asphalt Mixture.

Buildings **2023**, *13*, 16. <https://doi.org/10.3390/buildings13010016>

Academic Editor: Oldrich Sucharda

Received: 2 November 2022

Revised: 8 December 2022

Accepted: 16 December 2022

Published: 21 December 2022



Copyright: © 2022 by the authors. Licensee MDPI, Basel, Switzerland. This article is an open access article distributed under the terms and conditions of the Creative Commons Attribution (CC BY) license (<https://creativecommons.org/licenses/by/4.0/>).

1. Introduction

Steel slag is one of the major by-products in a metallurgical industry. The steel slag sold on the market each year, generally Basic Oxygen Furnace (BOF) steel slag and Electric Arc Furnace (EAF) steel slag, accounts for about 10–15% of steel production (by weight) [1]. Although the global economy has been negatively affected by COVID-19 pandemic, it should be noticed that 1.065 billion tons of steel were produced in China, which is 56.71% of global production. In the post COVID-19 period, it is expected that construction activities will increase, and manufacturing conditions will improve. With the recovery of the global economy, the demand and production of various machinery will increase, and the amount of metal products will increase as well, thereby driving the demand for more steel products. For instance, according to “Steel-Global Market Trajectory & Analytics”, it is estimated that China will produce 1.3 billion tons of steel by 2026 [2]. However, the recycling rate of steel slag is only 30% in China [3,4]. The steel slag, which is dumped in landfills, not only causes serious environmental pollution but also is a huge economic waste [5].

At present, steel slag is commonly used in pavement engineering, metallurgy, purification systems, fertilizer manufacturing and other fields. Among them, the common application of steel slag in pavement engineering is as coarse aggregate [6,7]. For example,

due to its natural wear resistance, steel slag can be used as a high wear-resistance pavement material [8]. Wu investigated the effect of steel slag as aggregates on the physical, chemical and mechanical properties of stone mastic asphalt (SMA) mixtures [9,10]. In another of his studies, the functional and environmental performances of a chip seal using recycled steel slag was evaluated [11]. The results indicate that steel slag can be used as aggregate in SMA mixtures and chip seals, instead of dumping in landfills, to eliminate the pollution risk. Oluwasola [12] and Liapis [13] found that pavement contains electric arc furnaces (EAF) slag has the higher skid number (British Pendulum Number, BPN) and mean texture depth than the conventional pavement. Hanin et al. found that various mixtures with steel slag have better rutting resistance than the common mixtures based on the results of creep tests [12–14]. Moreover, some researchers also found that the addition of steel slag coarse aggregate in asphalt mixture would improve the mechanical properties, [14,15] increase the fatigue life [16,17], improve the noise reduction of asphalt mixture [18]. All of the above studies demonstrate the potential of steel slag as an alternative aggregate in road materials.

However, the volume expansion potential of steel slag, as the main limitation to its wide use in asphalt pavement, still needs to be concerned. The current studies mostly attribute the volume expansion of steel slag to the hydration of free calcium oxide (f-CaO) [19,20]. Therefore, it is generally agreed that steel slag requires a stabilization period (i.e., aging, weathering) prior to use to facilitate the hydration of f-CaO, the process is essential for the preparation of high-quality aggregates. But previous researches have proved that aging or weathering treatments would alter the surface morphology of steel slag, and consequently adversely affect the road performance of steel slag based asphalt mixture, especially for moisture susceptibility [21]. For instance, Hesami et al. found that the use of EAF slag as fine aggregate significantly increase the moisture sensitivity of asphalt mixture [22]. Coomarasamy and Walzak found that chemical changes took place on the surface of steel slag when steel slag based asphalt mixture was in moist environment. The chemical changes resulted in poor moisture damage resistance of steel slag asphalt pavement [23].

Based above, improving the surface characteristics of steel slag aggregate (SSA) and strengthening the bonding of SSA and bitumen are critical to reduce the moisture damage of asphalt mixtures. Many studies have focused on the adhesion between SSA and bitumen. Chen et al. investigated the bonding behavior between basic oxygen furnaces (BOF) slag and bitumen. The result illustrated that BOF slag had better bonding strength with bitumen than that of the conventional aggregates [24]. Kambole et al. found that slag-bitumen mixtures show better stripping resistance than the mixtures with natural aggregates and SSA can be a high-quality substitute for natural aggregate [25]. Qazizadeh et al. founded that the bitumen has a stronger adhesion with steel slag than it with limestone, which leads to the improvement of fatigue property [26]. While these studies ignore the fact that the interaction between the binder and SSA is much more influenced by the surface properties of SSA than by the binder's own properties. Aggregates with the same physical and mechanical properties may show variations in adhesion due to differences in the chemical composition associated with the interaction forces formed between these materials [27,28]. Moreover, it is still very difficult to accurately and quantitatively evaluate the bonding properties of bitumen-SSA by experimental methods. On the other hand, there are relatively mature processes for surface treatment of SSA to achieve improvement of its surface properties. Ma et al. proposed a surface treatment method to block off surface voids and reduce the absorption amount of bitumen by steel slag [4]. Chen found that the BOF slag, which is pretreated by hydration and silicone resin, has a lower bitumen absorption and improve the resistance of volume expansion [29]. However, these studies mostly focus on the improvement on the surface pore and binder absorption of SSA, and fail to study the effect of surface pretreatment on the bitumen-SSA adhesion system, i.e., the improvement mechanism of surface pretreatment on the road performance of SSA asphalt mixtures has not been clarified.

This study aims to obtain pretreated SSA (PSSA) by surface treatment technology, investigate the effect of pretreatment process on the properties of SSA (surface morphology, chemical composition and swelling characteristics) and SSA-bitumen interface adhesion. Based on the surface free energy theory, the quantitative comparative evaluation of the adhesion between bitumen and five different types of aggregates (i.e., limestone, diorite, diabase, SSA, PSSA) was achieved by combining the contact angle test and BBS test. Furthermore, the pavement performance of hot asphalt mixtures (HMA) with limestone, SSA and PSSA was evaluated by Marshall stability test, wheel-tracking rutting test, low-temperature bending creep test and water sensitivity test.

2. Materials and Methods

2.1. Raw Materials

The SSA (EAF slag) was supplied by Jiangsu Binxin iron and Steel Group Co., Ltd., which has been crushed and aged for more than half of a year. PEN 60/80 bitumen, limestone aggregates and fillers are commonly used as pavement materials in northern China and are provided by local companies in Shanxi Province, China. Tables 1 and 2 present the specifications of studied materials, i.e., bitumen and aggregate. In addition, a gel agent (HC-1) was used to treat the surface of steel slag and its main chemical components (according to the recommendation of supplier) are shown in Table 3.

Table 1. Specifications of bitumen before and after short-term aging by rolling thin film ovens (RTFOT).

| Property | Unit | Value | Requirement | Test Method |
|------------------------------------|-------------------|-------|-------------|-------------|
| Penetration (25 °C, 100 g, 5 s) | 0.1 mm | 68 | 60~80 | T0604-2011 |
| Penetration index (PI) | - | -0.6 | -1.5~+1.0 | T0604-2011 |
| Softening point | °C | 46.0 | ≥45 | T0606-2011 |
| Ductility (10 °C) | cm | 31 | ≥20 | T0605-2011 |
| Ductility (15 °C) | cm | >100 | ≥100 | T0605-2011 |
| Wax content | % | 1.8 | ≤2.2 | T0615-2011 |
| Flashing point | °C | 310 | ≥260 | T0611-2011 |
| Dynamic viscosity (60 °C) | Pa·s | 200 | ≥160 | T0620-2000 |
| Density | g/cm ³ | 1.045 | - | T0603-2011 |
| RTFOT—mass loss | % | -0.25 | ≤±0.8 | T0610-2011 |
| RTFOT—Residual Penetration (25 °C) | % | 68 | ≥61 | T0604-2011 |
| RTFOT—Ductility (10 °C) | % | 7 | ≥6 | T0605-2011 |

Table 2. Specifications of SSA, PSSA and limestone aggregate.

| Property | SSA (Coarse) | PSSA (Coarse) | Limestone Aggregate (Coarse) | Limestone Aggregate (Fine) | Requirement | Test Method |
|---------------------------------------|-----------------|------------------|------------------------------------|----------------------------------|-------------|----------------|
| Apparent density (g/cm ³) | 3.482 | 3.525 | 2.727 | 2.699 | ≥2.60 | T0304-2005 |
| Water absorption (%) | 1.88 | 1.04 | 0.68 | - | ≤2 | T0304-2005 |
| Crush value (%) | 14.8 | 13.5 | 16.6 | - | ≤26 | T0316-2005 |
| Abrasion value (%) | 8.0 | 7.2 | 22.3 | - | ≤28 | T0317-2005 |
| Flakiness and elongation (%) | 2.2 | 2.2 | 7.5 | - | ≤12 | T0312-2005 |
| Sand equivalent (%) | - | - | - | 75 | ≥60 | T0334-2005 |

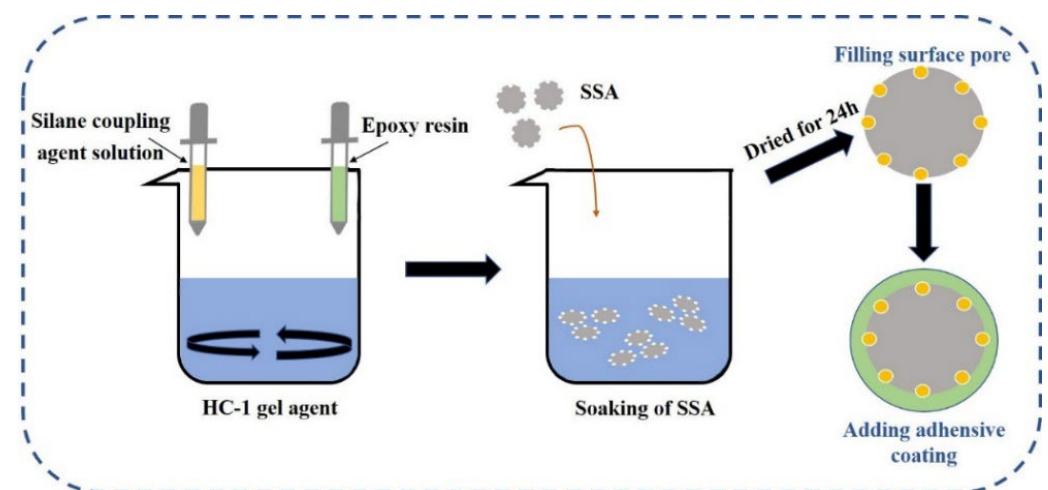
Table 3. Chemical compositions of HC-1 gel agent.

| Chemical Composition | Mass Fraction (%) |
|------------------------|-------------------|
| Anhydrous ethanol | 30~50 |
| Epoxy resin | 10~20 |
| Silane coupling agent | 5~10 |
| M-Xylylenediamine | 5~10 |
| Methyldiethanolamine | 3~5 |
| Liquid silicone rubber | 3~5 |

2.2. Surface Pretreatment of SSA

Previous studies had proved that the surface pretreatment of SSA with silane coupling agent could improve the adhesion of SSA to bitumen [29,30]. The surface pretreatment of SSA in this study is carried out by means of HC-1 gel agent, which is mainly composed of silane coupling agent and epoxy resin. The steps of the surface pretreatment of SSA are described below and shown in Figure 1:

1. To prepare the pretreatment agent, epoxy resin was solved in ethanol solution at a ratio of 3:10 by weight. Then, silane coupling agent (10 wt %), anhydrous ethanol (10 wt %), m-Xylylenediamine (14 wt %), methyldiethanolamine (8 wt %) and liquid silicone rubber (8 wt %) were added.
2. To pretreat the surface of SSA, it was immersed at 20 °C for 24 h in the agent which was prepared at the step (1).
3. Finally, PSSA were placed in an oven at 25 °C for 24 h which made agent to be fully cured.

**Figure 1.** Surface treatment of SSA.

2.3. Mixture Design

Based on Marshall Mix Design Method, the nominal maximum aggregate size of 13.2 mm was selected for HMA. HMA-limestone (HMA-L), HMA-SSA and HMA-PSSA were prepared. Except for coarse aggregate, they used the same materials, such as limestone fine aggregate and filler. The aggregate graduation of HMA-L, HMA-SSA and HMA-PSSA were shown in Figure 2.

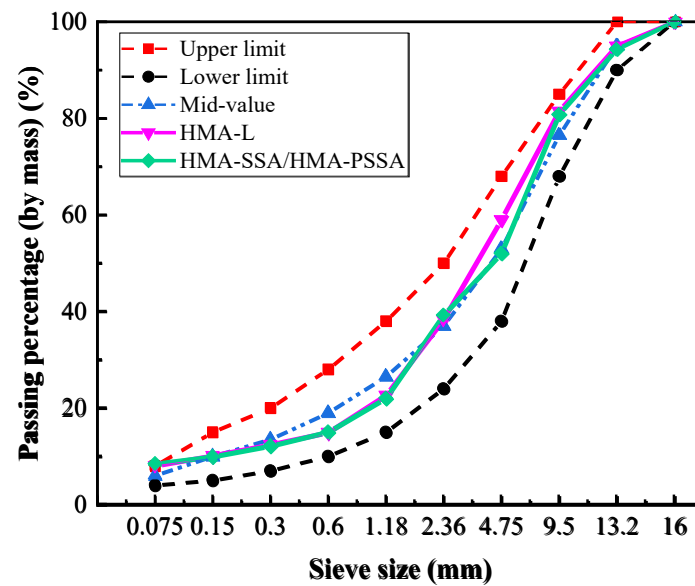


Figure 2. Gradation of three HMA.

2.4. Test Methods

2.4.1. Physical and Chemical Characterization of SSA

(a) Morphological test

Scanning electron microscope (SEM) was used to observe the surface texture and micro-pores of SSA, according to its imaging depth and three-dimensional characteristics. To be specific, 5 g dried SSA and PSSA particles were prepared and observed by a S-4800 cold field emission SEM.

(b) Mineral composition analysis

The mineral composition of SSA was determined by using the X-ray fluorescence (XRF). In addition, the alkalinity modulus (M) of SSA was calculated based on the ratio of acid and alkaline mineral content, and can be determined using Equation (1).

$$M = \frac{W_{\text{CaO}} + W_{\text{MgO}} + W_{\text{Fe}_2\text{O}_3}}{W_{\text{SiO}_2}} \quad (1)$$

where, W_{CaO} , W_{MgO} , $W_{\text{Fe}_2\text{O}_3}$ and W_{SiO_2} represent the mass percentage of CaO, MgO, Fe_2O_3 and SiO_2 in SSA, respectively.

(c) Swelling test

The volume stability of SSA and PSSA was evaluated by measuring the immersion volume expansion rate. In standard GB/T 24175-2009 (GB, 2009), slag samples (about 7 kg) were mixed with water and compacted in the mold, and then put into a water bath. After completely immersed, the gauge value (d_0) of the dial indicator was recorded on the top plate of the mold. And then the samples were heated and kept in a $(90 \pm 3)^\circ\text{C}$ water bath for 6 h. After cooling to the room temperature, the values of the dial gauge were recorded every 1 d for 10 d. Finally, the immersion volume expansion rate (δ) could be defined using Equation (2):

$$\delta_i = \frac{d_i - d_0}{120} \times 100\% \quad (2)$$

where, δ_i is the immersion expansion rate after i days immersed in water, %; d_0 is the initial value gauged by the dial indicator; d_i is the gauge value after i days immersed in water, 120 is the initial height of the test mold (mm).

2.4.2. Bitumen-Aggregate Adhesion Analysis

(a) Contact angle test

The concept of contact angle had been applied in many studies to verify the surface wettability of materials and thus to characterize the adhesion of solid-liquid interface [31–33]. In this study, lying drop method was used to test adhesion work between bitumen and five types of aggregates (i.e., limestone, diorite, diabase, SSA, PSSA). Bitumen was melted and solidified on the surface of a glass slide to form a flat solid surface. Three probe liquids with known surface energies, including distilled water, glycerol and formamide, which were insoluble in bitumen and do not react chemically with bitumen, were used to quantify the surface free energy of bitumen. The difference in surface wettability of different aggregate were identified by putting a drop of melted bitumen on the aggregate surface. During the test, images of the different liquid droplets on the solid surface were obtained by charge-coupled device (CCD) camera, and the contact angle were measured automatically.

(b) Binder Bond Strength (BBS) test

The BBS test was used to quantify the pulling force that needed to remove a pull stub attached to a solid substrate with bitumen. All aggregates were polished to minimize the influence of surface roughness on the test results (Figure 3). The preheated bitumen was poured into a silicone mold to form a disk sample with a diameter of 8 mm and thickness of 2 mm from AASHTO TP91. Finally, a pneumatic load was applied to a pull stub using an ASTM D 4541 Type IV adhesion tester (Figure 4) until adhesive failure at a temperature of 25 °C and a relative humidity of 45%. The pullout tensile strength and mode of failure were recorded during the tests.



Figure 3. Aggregate samples for BBS test.



Figure 4. ASTM D 4541 Type IV adhesion tester.

2.4.3. The Performance Evaluation of Asphalt Mixture

Firstly, according to the gradation in Figure 3, the optimum bitumen content (OAC) of three bituminous mixtures (HMA-L, HMA-SSA and HMA-PSSA) were determined.

Further, standard Marshall test, wheel-tracking rutting test, low-temperature bending creep test, and freeze-thaw spitting test were conducted according to the Chinese standard of JTG E20-2011 to evaluate the performance of three mixtures.

3. Results and Discussion

3.1. Surface Structure and Pore Changes of SSA

The SEM images of SSA, PSSA and limestone at a magnification of $400\times$ were presented in Figure 5. It can be seen in Figure 5a that the SSA had a rough surface with numerous pores and micro-cracks, while the surface of the limestone was smooth with few pores (Figure 5b). To be specific, the diameter of the pore was about $100\text{ }\mu\text{m}$ and length of the micro-crack was about $20\text{ }\mu\text{m}$ on the SSA surface (Figure 5a). Generally, it was believed that an aggregate with porous and rough surface potentially had an excellent physical adhesion with bitumen due to its larger contact area [34]. However, excessive pores would increase the water absorption of the aggregate, thereby reducing the water stability of the asphalt mixture [8]. Additionally, it can be noticed from Figure 5a that these large pores densely distributed inside SSA and micro-cracks would be formed at the contact area between SSA and SSA. The existence of micro-cracks will greatly increase the risk of cracking damage of HMA-SSA during its service life.

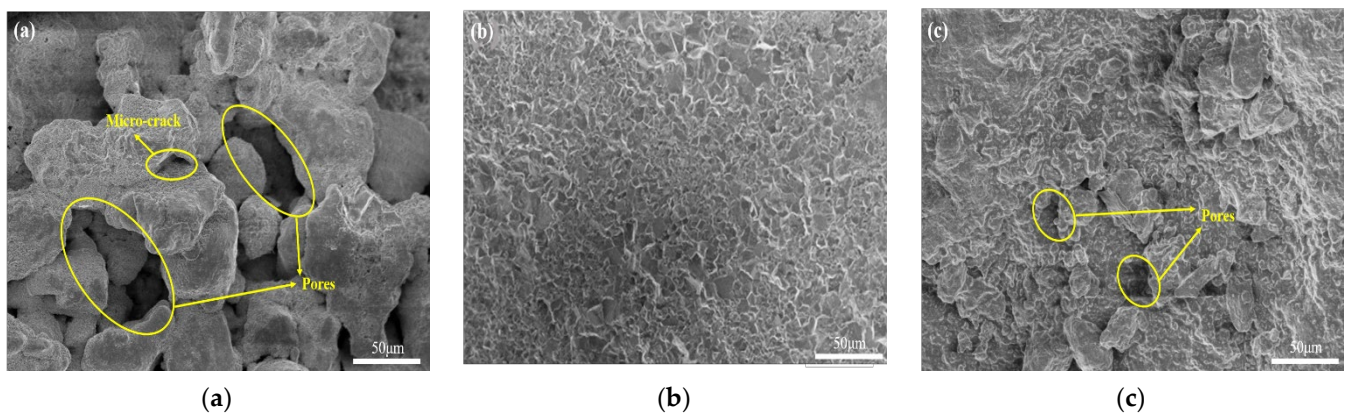


Figure 5. SEM images: (a) SSA magnified 400 times; (b) Natural limestone magnified 400 times; (c) PSSA magnified 400 times.

Figure 5c showed that the surface of PSSA smoother than that of SSA, because the large pores on the SSA surface were filled by gel agent. In the meanwhile, it can be observed that there were still a certain number of small pores with a size about $40\text{ }\mu\text{m}$ on the surface of PSSA, which ensured that it has a sufficient adhesive area with bitumen [29]. In addition, the filling gel agent made the whole coating of PSSA to be more complete without the blind areas compared to SSA. So the gel agent can be considered as a protective layer, which leads to a reduced risk of water penetration into the interior of the PSSA. Overall, it can be concluded that surface pretreatment of SSA can effectively improve the performance of HMA-SSA by reducing the water corrosion and improving its adhesion to bitumen.

In order to quantitatively evaluate the surface defects of SSA, limestone and PSSA, SEM images of the three aggregates were processed by digital-image method. Firstly, the images were binarized according to the differences in gray values of pores, micro-cracks and aggregate. Then the pixel area statistics function in the Image Pro Plus (IPP) 6.0 software was used to calculate the pixel area of the surface defects and the entire sample area, and the average calculated value of the area ratio was selected as the evaluation index, the results are shown in Figure 6. It can be clearly seen that the pores and microcracks of limestone are only 0.12% and 0.05%, which are much less than SSA and PSSA, and can be approximated as a dense material. In terms of PSSA, it can be noted that the filling of the gel agent leads to pores and micro-cracks on the surface of SSA reduced by 6.65% and 2.56%, respectively, which demonstrates the surface improvement results of PSSA.

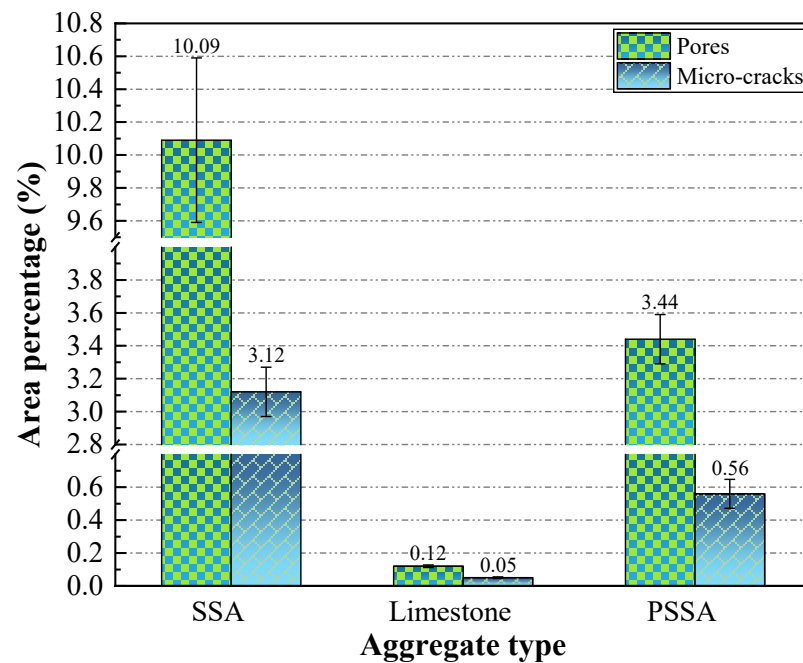


Figure 6. >The pores and micro-cracks area percentage of SSA and PSSA.

3.2. Chemical Composition of SSA

The main chemical compositions of SSA, which were measured by X-ray fluorescence spectrometer, were shown in Table 4. It was noted that SiO_2 , Fe_2O_3 , MgO and CaO were the main mineral components of SSA. Among them, the content of CaO was the highest, which was 35.79 wt%, followed by Fe_2O_3 and SiO_2 which was 20.31 wt% and 20.04 wt%, respectively. The alkalinity modulus results for the individual aggregates obtained from Equation (1) are shown in the Table 5. It can be clearly seen that SSA and limestone are alkaline aggregates (M value > 1), diorite and diabase are acidic aggregates (M value < 0.6), and SSA exhibits a weaker alkalinity than limestone.

Table 4. The chemical compositions of SSA.

| Components | Content/wt% |
|-------------------------|-------------|
| CaO | 35.79 |
| Fe_2O_3 | 20.31 |
| SiO_2 | 20.04 |
| MgO | 8.53 |
| Al_2O_3 | 3.00 |
| MnO | 2.18 |
| P_2O_5 | 1.46 |
| TiO_2 | 0.56 |
| K_2O | 0.54 |
| Na_2O | 0.46 |
| OTHER | 7.13 |
| TOTAL | 100.00 |

Table 5. Comparison of alkalinity modulus between SSA and other aggregates.

| Aggregate Type | Limestone | Diorite | Diabase | SSA |
|----------------------------|-----------|---------|---------|------|
| Alkalinity modulus (M) | 5.45 | 0.09 | 0.35 | 3.22 |

3.3. Swelling Properties of SSA

Figure 7 presented the swelling results of SSA and PSSA at different immersion periods. It was found that the swelling of SSA increases with immersion time, which

was mainly caused by the volume expansion of free calcium oxide and magnesium oxide in SSA during immersion. The existence of a high proportion of unstable free oxides in SSA would degrade the mechanical properties of asphalt mixture under water condition, thereby reducing the durability of asphalt pavement and affecting driving safety [35]. In addition, it's worth noting that the volume expansion rate of PSSA was significantly smaller than that of SSA at the same soaking age, and the volume expansion behavior of PSSA lasted shorter, reaching the end time on the 8th day. This proves that PSSA is superior to SSA in volume stability, which may be related to the water resistance ability of the organic coating on the surface. Although the volume expansion of SSA continues to increase with the immersion time, it needs to be pointed out that the slope of volume expansion growth of SSA decreases significantly after the 9th day and the swelling rate of the SSA after 10 days immersion still met the requirement of current specification (swelling rate $\leq 2.0\%$, GB/T 25824-2010).

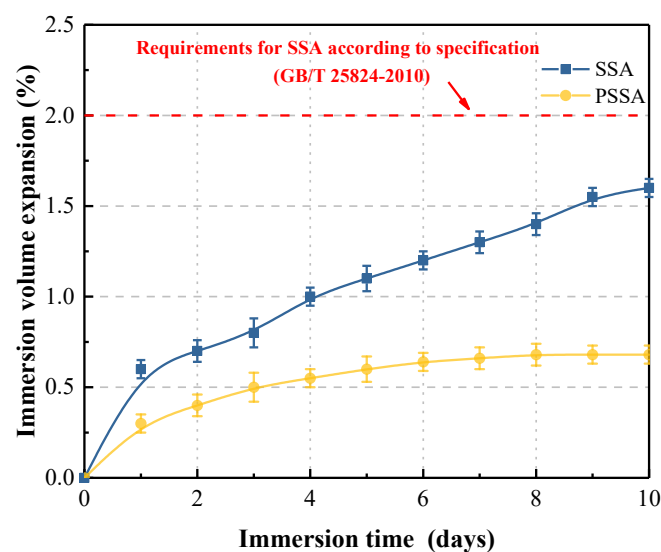


Figure 7. Swelling test results of SSA and PSSA.

3.4. Adhesion and Stripping Work

According to the surface energy theory, any substance tends to attract other molecules to reach its lowest energy state [36,37]. In the bitumen-aggregate system, the aggregate spontaneously attracts bitumen due to the force field of its surface, thus reducing the surface energy and forming a stable system. This theory can be used to quantitatively evaluate the different adhesion of bitumen with different types of aggregates. In the case of bitumen-aggregate-water system, under repeated moving vehicles, water entered the interface between bitumen and aggregate. Then the bitumen gradually lost adhesive at the interface between bitumen and aggregate. As a result, the bitumen peeled off from the aggregate surface. The adhesion work and stripping work were used to evaluate the adhesion of the binder-aggregate interface and the extent of water resistance of asphalt mixture.

The surface energy of bitumen can be calculated using Equations (3) and (4) which can be obtained from the Young equation [25] and surface energy theory [38].

$$\gamma_l(1 + \cos \theta) = 2\sqrt{\gamma_s^p \gamma_l^p} + 2\sqrt{\gamma_s^d \gamma_l^d} \quad (3)$$

$$\gamma_l = \gamma_l^d + \gamma_l^p \quad (4)$$

where, γ_l^d and γ_l^p express the dispersion component and polar component of the surface energy of liquid. γ_s^p and γ_s^d are the dispersion component and polar component of the

solid in vacuum respectively. The contact angle (θ) is the angle connecting the bitumen-probe liquid interface.

The adhesion work and stripping work can be calculated using Equations (5) and (6):

$$W_{a-g} = \gamma_w(1 + \cos \theta) \quad (5)$$

$$W_{a-s-w} = \gamma_{s-a} - \gamma_{a-w} - \gamma_{s-w} = \gamma_w(1 + \cos \theta_1) + \gamma_w(1 + \cos \theta_2) - \gamma_a(1 + \cos \theta_3) \quad (6)$$

where, W_{a-g} and W_{a-s-w} are the adhesion work and stripping work of bitumen and aggregate, γ_{s-a} , γ_{a-w} and γ_{s-w} represent the interface energies of asphalt-aggregate, asphalt-water and aggregate-water respectively, and the corresponding contact angles are marked as θ_3 , θ_2 and θ_1 .

Table 6 showed the surface free energy of bitumen and the three probe liquids. The surface energy data of bitumen was obtained by substituting the surface energy parameters of the probe liquid and the bitumen-probe liquid contact angle shown in Figure 8 into Equations (3) and (4). The adhesion and stripping work of all the aggregates were obtained by using Equations (5) and (6) from the data of contact angle in Figures 9 and 10, and the results are presented in Table 7.

Table 6. Surface free energy of bitumen and probe liquid (mJ/m²).

| Reagent | γ^d | γ^p | γ |
|-----------------|------------|------------|----------|
| Distilled water | 21.8 | 51.0 | 72.8 |
| Glycerol | 34.0 | 30.0 | 64.0 |
| Formamide | 39.0 | 19.0 | 58.0 |
| Bitumen | 29.1 | 0.37 | 29.47 |

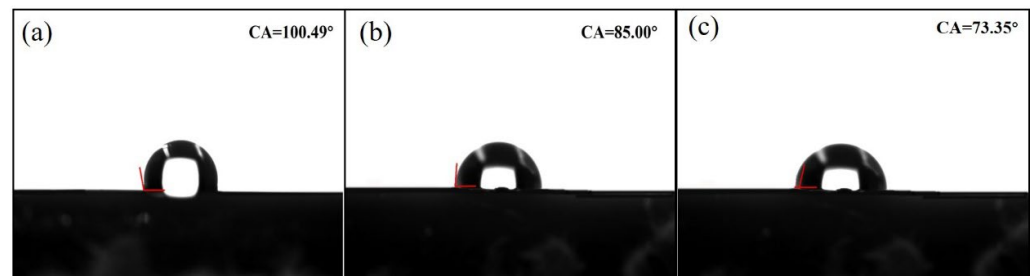


Figure 8. Contact angle of bitumen with probe liquid: (a) distilled water; (b) glycerol; (c) formamide.

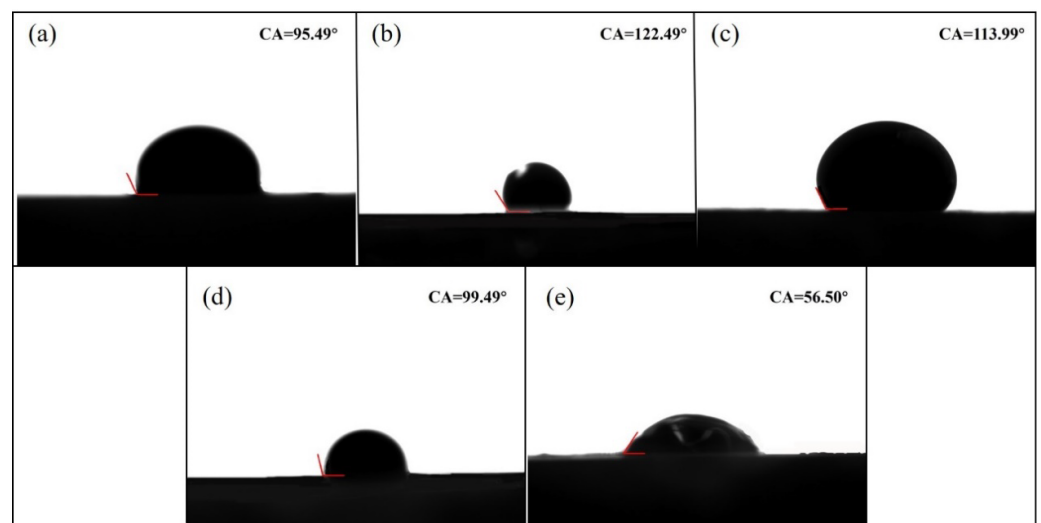


Figure 9. Contact angle of bitumen with aggregates: (a) limestone; (b) diorite; (c) diabase; (d) SSA; (e) PSSA.

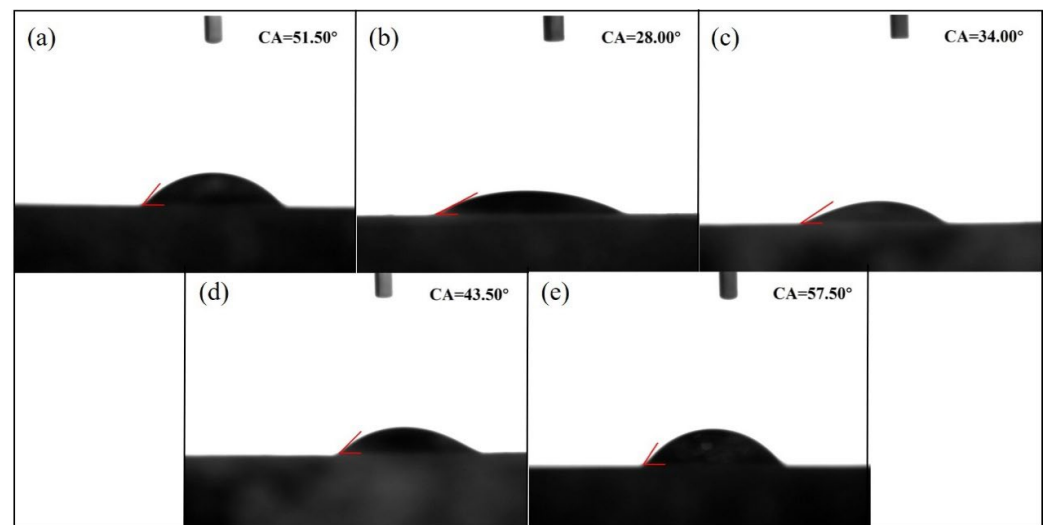


Figure 10. Contact angle of water with aggregates: (a) limestone; (b) diorite; (c) diabase; (d) SSA; (e) PSSA.

Table 7. Adhesion work and stripping work of various aggregates and bitumen (mJ/m^2).

| Aggregate Category | Adhesion Work (W_{a-g}) | Stripping Work (W_{a-s-w}) |
|--------------------|-----------------------------|--------------------------------|
| Limestone | 26.65 | 151.01 |
| Diorite | 13.64 | 182.98 |
| Diabase | 17.49 | 175.21 |
| SSA | 24.61 | 160.54 |
| PSSA | 45.74 | 125.73 |

The value of W_{a-g} represents the bitumen-aggregate interface strength, while the W_{a-s-w} reflects the moisture damage that occurs at the bitumen-aggregate interface. The high value of W_{a-g} and the low value of W_{a-s-w} indicated higher bond strength and good moisture damage resistance of bitumen-aggregate system [36]. As can be seen from Table 7, the adhesion work of SSA is lower than that of limestone, while it is much higher than that of diorite and diabase. Moreover, the value of stripping work exhibits exactly the opposite results. These results indicated that in terms of the same bitumen, moisture damage resistance of SSA is better than that of diorite and diabase, and slightly lower than limestone. This can be attributed to the different alkalinity of aggregates. The alkaline limestone and the acidic bitumen have relatively high polarity, resulting in the bitumen-limestone has high bond strength and water stability. In addition, it can be noticed that PSSA has the highest W_{a-g} value and the lowest W_{a-s-w} value in Table 7. This is mainly because the highly hydrophobic nature of HC-1 gel agent coating, which improves the SSA surface properties, increased the contact angle from 43.50° (Figure 10d) to 57.50° (Figure 10e). It denotes that the adhesion between bitumen and PSSA is higher than it with SSA, due to hydrophobic surface of PSSA. In another word, the increased hydrophobicity during the surface treatment, can prevent water to damage the interfaces with PSSA and bitumen.

3.5. Binder Bond Strength

In BBS test, the pull-out strength is defined as the tension required to remove the pull-out nipple attached to the prefabricated surface by applying tension in the normal direction with bitumen. The corresponding pull-out failure can occur at two locations: within the bitumen or at the bitumen and substrate interface, examples are provided in Figure 11. The failure within bitumen, also known as cohesive failure, is mainly caused by the weakening of the bitumen properties, while the failure between bitumen and aggregate interface (adhesion failure), was caused by the reduction of the adhesion between bitumen

and aggregate due to the loss of bitumen film at the interface. In this test, test results of the adhesion failure mode were selected for evaluating tensile strength between bitumen and different aggregates, such as Figure 11b.



Figure 11. Examples of Bond strength Testing Failure Modes for bitumen-aggregate system: (a) Failure within the binder, (b) Failure at the binder/substrate interface.

The pull-off tensile strength of different aggregates were as shown in Figure 12. It was worth noting that limestone possesses the highest pull-off tensile strength, followed by diorite and diabase among the natural aggregates, which was highly consistent with the results of alkalinity modulus of the three aggregates mentioned in previous content. Besides, the pull-off tensile strength of SSA was higher than that of diorite and diabase but lower than that of limestone, which was related to the lower alkalinity modulus of SSA, but it illustrated that the adhesive strength of PSSA and bitumen was significantly higher than that of other aggregates. This phenomenon further proved that a better adhesion can be achieved between an acidic binder and PSSA due to surface treatment.

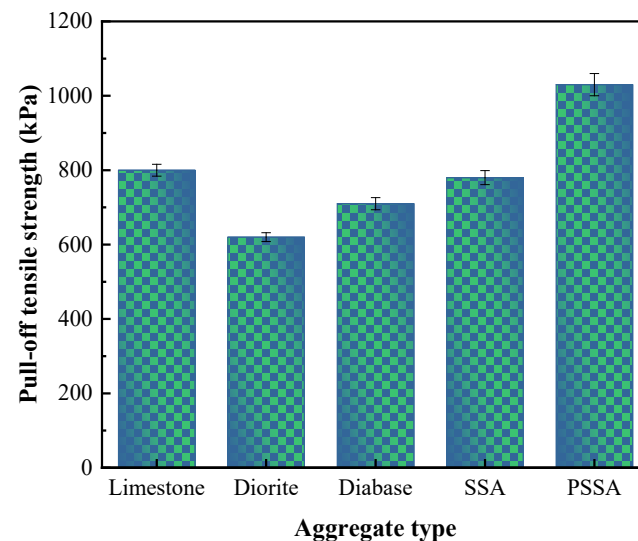


Figure 12. BBS test results.

To correlate the results from BBS test and surface energy test, the adhesion work and stripping work of various aggregate types were fitted with the pull-off tensile strength, and the results are shown in Figure 13. As expected, a good correlation could be observed between the BBS test results and the surface energy [39]. To be specific, it is noteworthy that higher pull-off tensile strength implies higher adhesion work and lower stripping work, and the correlation coefficient are 0.99 and 0.97 respectively. The correlation suggested that BBS test results and surface properties of different bitumen-aggregate system are generally in agreement.

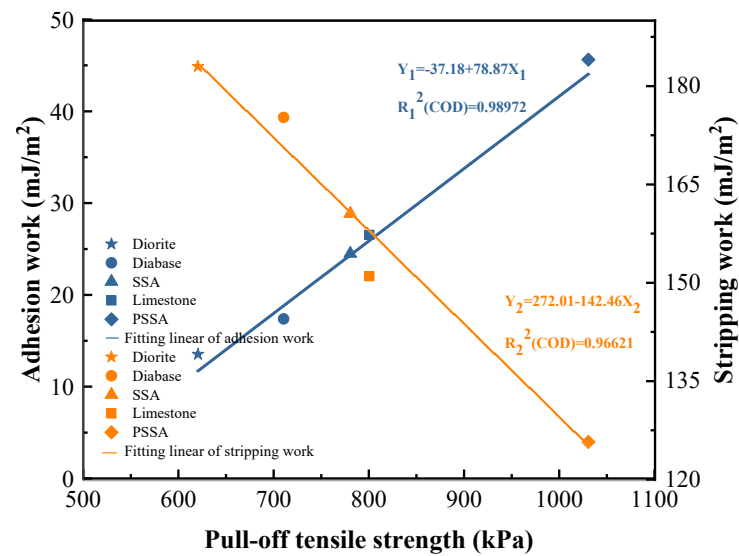


Figure 13. Fitting curves of drawing strength with adhesion work and stripping work.

3.6. Pavement Performance of Asphalt Mixture

3.6.1. Standard Marshall Test

The optimal bitumen content of HMA-L, HMA-SSA and HMA-PSSA mixtures were obtained by the curve of bitumen-aggregate ratio and various volumetric and mechanical indices of the mixture (Figure 14) based on the standard Marshall tests. The values of bitumen-aggregate ratio correspond to the maximum gross volume relative density, maximum stability, average porosity, and average saturation of HMA-SSA were recorded as a_1 , a_2 , a_3 and a_4 , respectively, as shown in Figure 14. Initial value of optimum bitumen content (OAC_1) was determined by Equation (7).

$$OAC_1 = (a_1 + a_2 + a_3 + a_4) / 4 \quad (7)$$

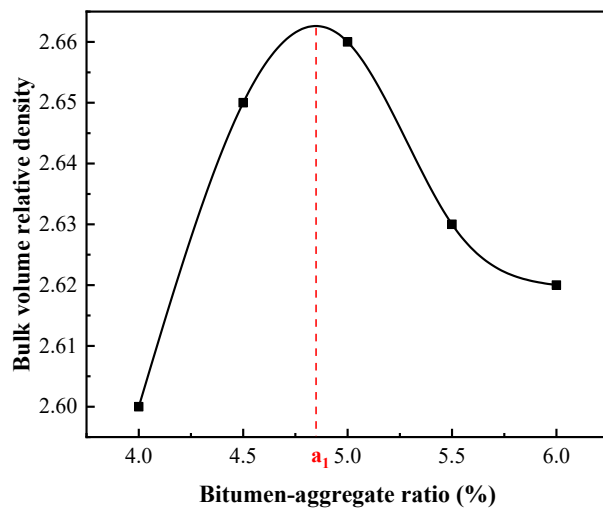
Then, the common range $OAC_{min} \sim OAC_{max}$ of all volume parameters meeting the requirements of the specification was determined and the average value of them was denoted as OAC_2 . The optimal bitumen content (OAC) was the mean value of OAC_1 and OAC_2 . And the same method was applied to calculate the OAC of HMA-L and HMA-PSSA. All the OAC were presented in Table 8 and the ultimate test results of design mixtures were shown in Table 9.

Table 8. OAC results for mixtures.

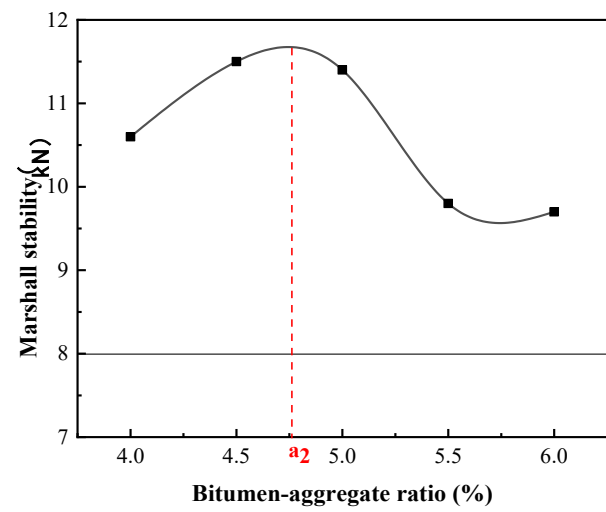
| Mixture Type | Bitumen Content (%) | | | | |
|--------------|---------------------|-------------|-------------|---------|-------|
| | OAC_1 | OAC_{min} | OAC_{max} | OAC_2 | OAC |
| HMA-L | 5.18 | 4.50 | 4.80 | 4.65 | 4.92 |
| HMA-SSA | 5.12 | 5.00 | 5.75 | 5.37 | 5.25 |
| HMA-PSSA | 5.20 | 4.00 | 5.75 | 4.87 | 5.04 |

Table 9. Marshall test results.

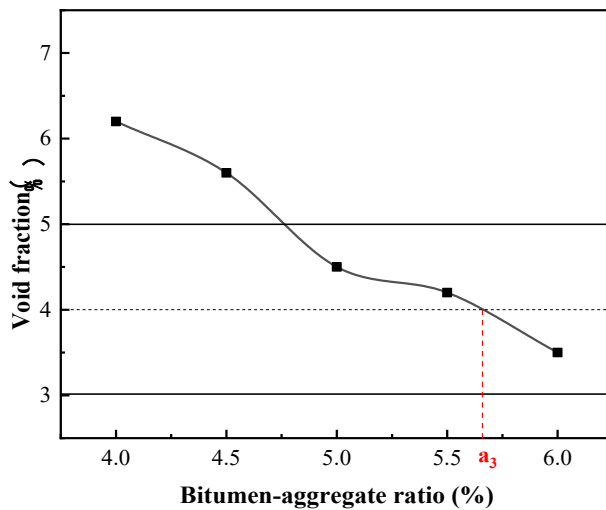
| Mixture Specimen | Marshall Parameter | | | | | | |
|--------------------------|----------------------|--------|---------|---------|---------|---------|-----------|
| | Bulk Density (g/cm³) | VV (%) | VMA (%) | VFA (%) | MS (kN) | FL (mm) | T (kN/mm) |
| HMA-L | 2.433 | 4.5 | 14.42 | 68.79 | 11.79 | 3.60 | 3.275 |
| HMA-SSA | 2.487 | 4.9 | 14.81 | 66.91 | 10.45 | 3.61 | 2.895 |
| HMA-PSSA | 2.472 | 4.1 | 14.25 | 71.23 | 12.06 | 3.44 | 3.506 |
| Requirements (JTG, 2004) | / | 3–6 | ≥13.00 | 65–75 | ≥8 | 1.5–4.0 | / |



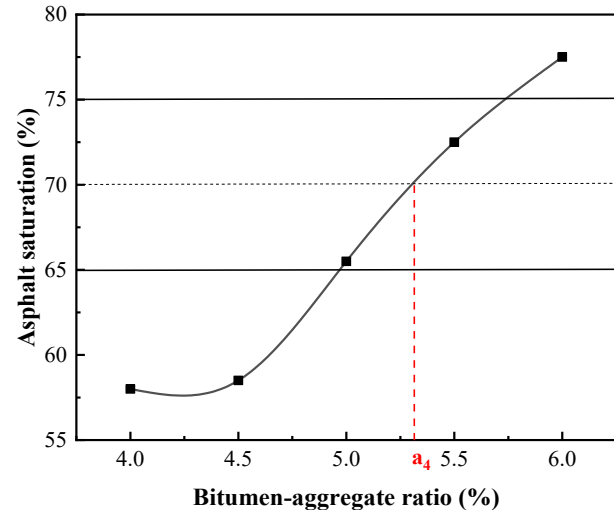
(a) Bulk volume relative density



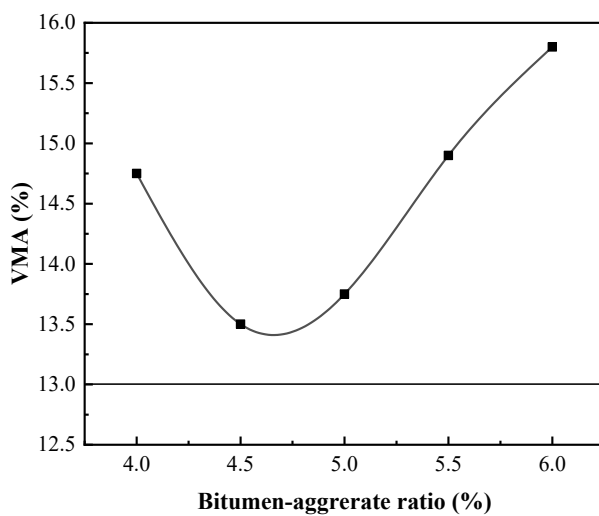
(b) Marshall stability



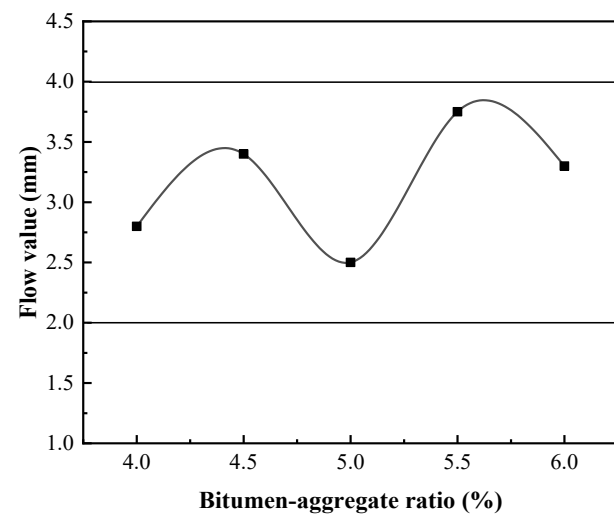
(c) Void fraction



(d) Asphalt saturation



(e) VMA



(f) Flow value

Figure 14. Relationship between volume parameters of HMA-SSA and bitumen-aggregate ratio.

Marshall stability (MS) represents the maximum load which same is carried before failure, and Flow value (FL) indicates the change in the diameter of the sample in the direction of load application between the start of loading and at the time of maximum load. In the standard Marshall test, specimens should be kept for 30–40 min in a 60 °C constant temperature water tank, and then tested under the load condition of a maximum load greater than 25 kN and a loading rate of 50 mm/min. As Table 9 displayed, the Marshall parameters of the three specimens all met the standard requirements. It can be noticed that HMA-SSA mixture showed the lowest MS and highest FL among the three mixtures, while the MS value of HMA-PSSA was significantly improved compared with that of HMA-SSA. In addition, the ratio of MS to FL, stated as the Marshall modulus (T), is an empirical indicator which is used to evaluate the resistance to shear stresses and creep deformation, and the T values of three mixtures are added in Table 9. Specifically, HMA-PSSA has the highest T value, which indicates it has a high stiffness and good resistance to permanent deformation.

3.6.2. Wheel-Tracking Rutting Test

Figure 15 presents the wheel-tracking test results of the three types of asphalt mixtures. And the dynamic stability (DS, conducted at 60 °C) was applied to evaluate the resistance to permanent deformation. It shows that three types of mixtures all have satisfactory high temperature stability ($DS \geq 1000$, according to specification, JTG F40-2004). Additionally, HMA-SSA and HMA-PSSA exhibited the similar deformation lower than that of HMA-L, which can be attributed to the fact that the tighter interlocking formed by the angular structure of SSA/PSSA particles [40,41]. In comparison, the average dynamic stability of HMA-PSSA is much higher than the other two types of mixtures under the same test conditions. This was because that HC-1 gel agent increased the strength of steel slag aggregate and reduced the bitumen content, both contributing to the high-temperature performance of the mixture. In one word, it suggests that HMA-PSSA performs better in rutting tests and can resist high temperature deformations at the same load level.

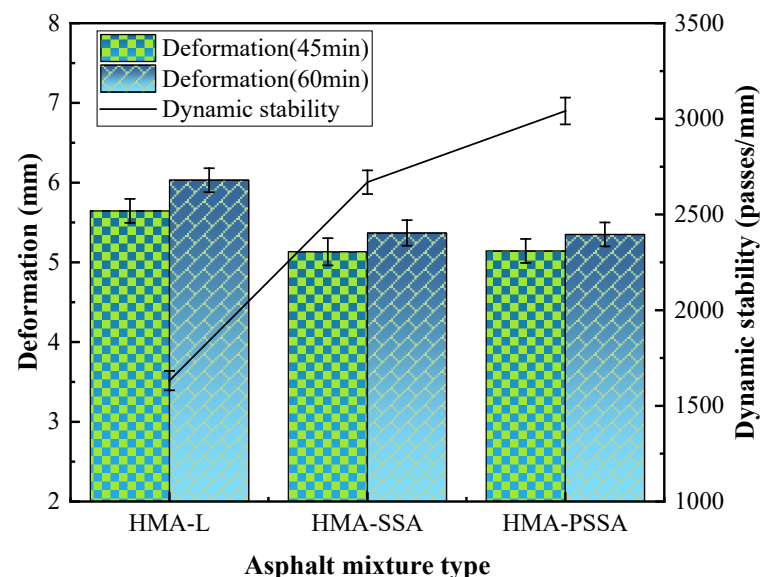


Figure 15. High-temperature stability and permanent deformation test results.

3.6.3. Low-Temperature Bending Creep Test

The low-temperature bending creep test was conducted at -10 °C and the loading rate was 50 mm/min. Figure 16 showed the comprehensive bending creep test results of HMA-L, HMA-SSA and HMA-PSSA. It can be concluded that all three mixtures can meet the requirement of the current pavement design specification (flexural failure strain $\geq 2000 \mu\epsilon$ for base asphalt mixture, according to specification, JTG F40-2004). Besides,

HMA-L has better crack resistance than HMA-SSA and HMA-PSSA because it has the maximum flexural strain. The flexural stiffness modulus and tensile strength of the three mixtures exhibited exactly opposite trends. This phenomenon proved that the existence of SSA\PSSA would slightly reduce the low-temperature flexural tensile performance of asphalt mixture.

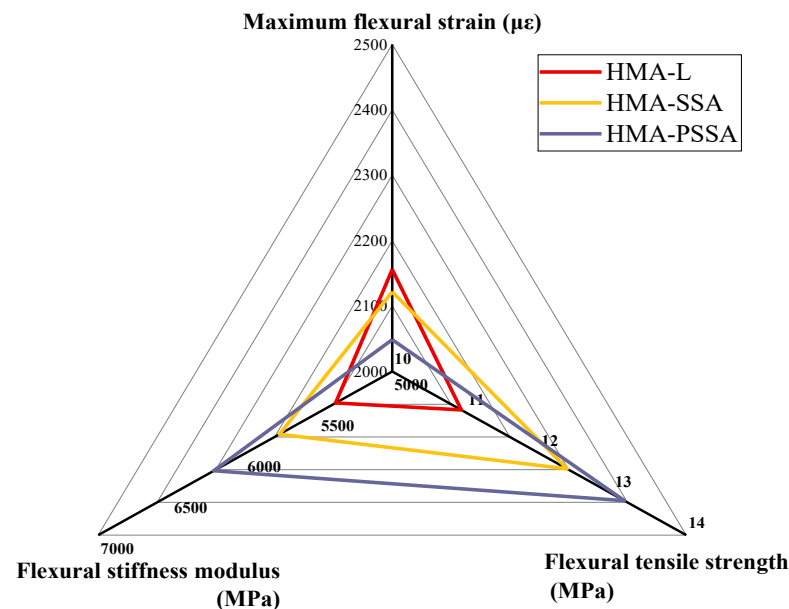


Figure 16. Low-temperature bending creep test results.

3.6.4. Immersion Marshall Test and Freeze-Thaw Splitting Test

In asphalt mixtures, the presence of water can corrode and weaken the bonding between bitumen and aggregate, which would cause the stone loss of the pavement surface and reduce the traffic safety. Immersion Marshall test and Freeze-thaw splitting test were applied to evaluate moisture damage resistance of three types of mixtures in this research, and the results are shown in Figures 17 and 18.

The results indicated that all mixtures had no obvious moisture-induced damage trend under the conditions of immersion and cyclic freeze-thaw since residual Marshall stability (MS) and their tensile strength ratio (TSR) all met the specification requirements (Residual MS ≥ 80 , TSR ≥ 75 , according to specification, JTG F40-2004). Furthermore, it was noteworthy that the residual stability of HMA-PSSA was significantly better moisture susceptibility than that of HMA-L and HMA-SSA in the immersion Marshall test. The moisture sensitivity of HMA-SSA is less than that of HMA-L, which is mainly because of the high porosity and roughness surface of SSA, and its affinity with bitumen [22,42]. On the other hand, the TSR values of HMA-SSA and HMA-PSSA were 9.4% and 11.2% higher than that of HMA-L respectively, exhibiting excellent freeze-thaw susceptibility. The higher porosity and roughness of slags, as well as the slightly higher OAC, resulting in a thicker coating of the SSA particles with bitumen and the improvement of freeze-thaw susceptibility of HMA-PSSA. Moreover, it could be seen that HMA-PSSA shows better moisture damage resistance than HMA-SSA, which demonstrates that the pre-treatment of SSA surface, that is given by HC-1 gel, enhances the bonding between aggregates and bitumen, and to improve moisture susceptibility.

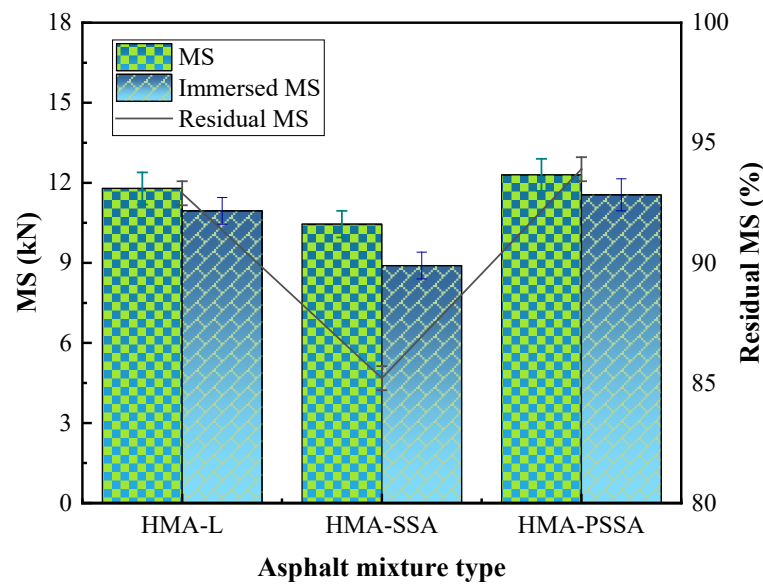


Figure 17. Immersion Marshall test results.

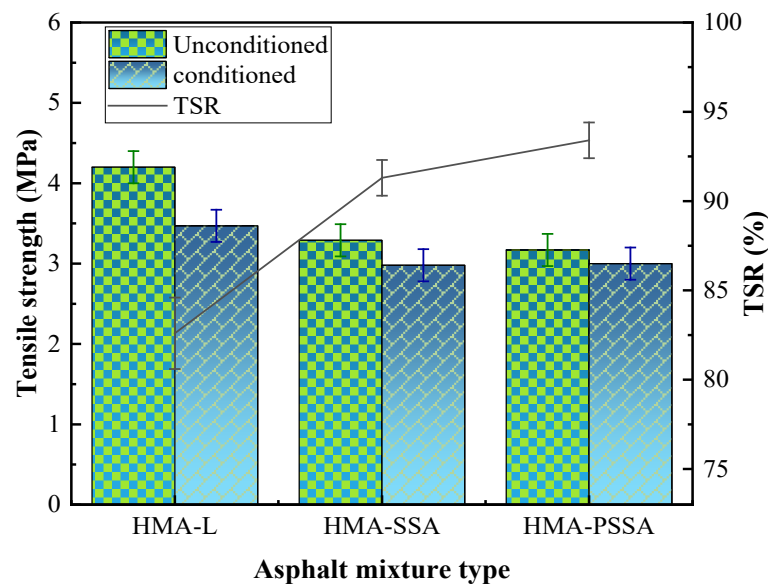


Figure 18. Freeze-thaw splitting test results.

3.6.5. Comprehensive Performance Analysis

In order to intuitively compare and analyze the road performance differences of the three asphalt mixtures, a series of road performance test results mentioned above were summarized, and the coupling effect of each road performance was plotted by selecting Marshall modulus (T), dynamic stability (DS), residual MS, flexural tensile strength, flexural stiffness modulus and tensile strength ratio (TSR) as axes, as shown in Figure 19a. It was obvious from the radar chart that HMA-PSSA has a significant dominance in the axial direction of DS, T, TSR and residual MS, but there is a notch along the axis of maximum bending strain. This indicated that it has the best road performance except low-temperature crack resistance. Additionally, the performance advantage of HMA-SSA appears primarily in the DS and TSR indices, and its low temperature performance is weaker than that of HMA-L and slightly better than HMA-PSSA. However, it is noteworthy that in terms of water stability, HMA-SSA exhibits a large fluctuation compared to HMA-L because of its higher TSR but lower residual MS.

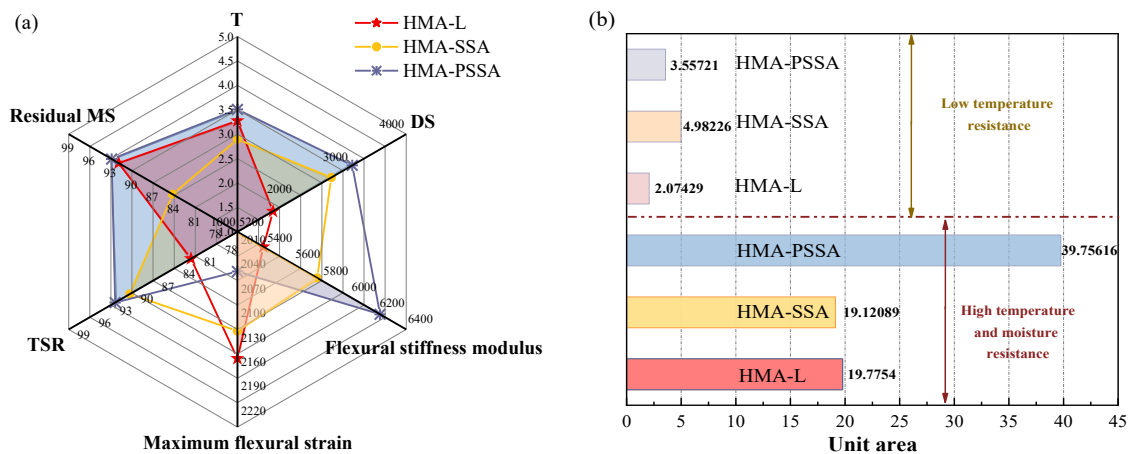


Figure 19. Comprehensive road performance of mixtures: (a) Coupling of road performance indicators; (b) Unit area.

Considering the inverse correlation of the low temperature index with performance and the inconsistency of the ranking exhibited by the three mixtures in each performance index, the area in Figure 19a is divided into two parts: the area enclosed by the axes of DS, T, residual MS and TSR (converted to grid cell area) is used as the comprehensive evaluation parameter of high temperature and moisture resistance; similarly, the area enclosed by the axes of maximum flexural strain and flexural stiffness modulus is used as the evaluation parameter of low temperature resistance, the corresponding unit area results are shown in Figure 19b. It can be seen that in terms of high temperature and moisture resistance, HMA-SSA and HMA-L perform equivalent, while HMA-PSSA is excellent, with approximately twice the unit area. For low temperature resistance, the superiority of the performance is inversely correlated with the value of unit area, it can be found from the results that the replacement of limestone with SSA improves the unit area by a multiple of 1.5, indicating an increase in low-temperature sensitivity. While the replacement of SSA with PSSA will make the increase in the unit area by a multiple of 0.7.

In a comprehensive comparison, surface pretreatment was beneficial to SSA as an alternative aggregate, which was significantly reflected in the high temperature deformation resistance and the significant improvement of residual MS of the mixture. Therefore, surface modified SSA could be used as a potential material for asphalt pavement design in high temperature and rainy areas.

4. Conclusions

This paper studies the influence of surface modification on the adhesive properties of PSSA. Marshall stability, dynamic stability, flexural failure strain, residual Marshall stability and tensile strength ratio were studied on HMA-L, HMA-SSA and HMA-PSSA. The conclusions can be drawn as follows:

1. The SEM results showed that the surface of SSA was rough, and there were micropores with a diameter of 100 μm and micro-cracks with a length of 20 μm . After surface treatment, PSSA still owned retained the rough surface structure and pores with size about 40 μm . PSSA have the better microstructure than SSA.
2. After the surface pretreatment of SSA, the adhesion of PSSA and bitumen was better than that of limestone and SSA. In addition, the BBS test results also confirmed this phenomenon and the correlation between pull-off tensile strength, adhesion work and stripping work were determined.
3. HMA-PSSA presented good Marshall stability and dynamic stability due to high adhesion of PSSA to bitumen. However, the low temperature performance of HMA-PSSA is not satisfactory, but it meets the corresponding requirements.

4. HMA-PSSA showed less moisture sensitivity than HMA-L and HMA-SSA in both immersion Marshall test and freeze-thaw splitting test. This explains that HMA-PSSA has better moisture damage resistance than HMA-L and HMA-SSA.

In summary, this study provides an alternative way for the recycling of steel slag and sheds a light on the practical value for the promising application of SSA in building materials. Further research is still needed particularly in terms of large scale practical application, economic feasibility and advantages of the pretreatment approaches and technology.

Author Contributions: Conceptualization, X.L.; methodology, D.N., Z.Y. and X.L.; validation, J.M.; data collection, Z.Z. and P.L.; data analysis, D.N. and Z.Z.; investigation, J.M. and Y.S.; resources, J.M. and Y.S.; writing—original draft, D.N. and Z.Z.; writing—review and editing, Z.Y., R.J., X.L. and P.L.; supervision, Z.Y. and R.J. All authors have read and agreed to the published version of the manuscript.

Funding: This work was supported by the Science and Technology Project of Henan Department of Transportation (No. 2020J-2-3), the China Scholarship Council (No. 202006565019) and the Fuzhou Science and Technology Bureau (2021-P-031), Shaanxi Housing and Urban-Rural Development Science and Technology Project (2020-K11).

Data Availability Statement: Data is available with the first author and can be shared with anyone upon reasonable request.

Conflicts of Interest: The authors declare that they have no known competing financial interest or personal relationships that could have appeared to influence the work reported in this paper.

References

1. Proctor, D.M.; Fehling, K.A.; Shay, E.C.; Wittenborn, J.L.; Green, J.J.; Avent, C.; Bigham, R.D.; Connolly, M.; Lee, B.; Shepker, T.O. Physical and chemical characteristics of blast furnace, basic oxygen furnace, and electric arc furnace steel industry slags. *Environ. Sci. Technol.* **2000**, *34*, 1576–1582. [CrossRef]
2. October, M. Global Steel Markets to 2026—Hit by COVID-19 Outbreak, Steel Industry & Demand Speedily Returning to Normalcy. 2021. Available online: <https://www.globenewswire.com/news-release/2021/10/06/2309315/0/en/Global-Steel-Markets-to-2026-Hit-by-COVID-19-Outbreak-Steel-Industry-Demand-Speedily-Returning-to-Normalcy.html> (accessed on 25 October 2022).
3. Le, K.; Hui, L.D.; Hao, Z.; Wan, L.M. Systematic research on the application of steel slag resources under the background of big data. *Complexity* **2018**, *2018*, 6703908. [CrossRef]
4. Ma, L.; Xu, D.; Wang, S.; Gu, X. Expansion inhibition of steel slag in asphalt mixture by a surface water isolation structure. *Road Mater. Pavement Des.* **2019**, *21*, 2215–2229. [CrossRef]
5. Guo, J.; Bao, Y.; Min, W. Steel slag in China: Treatment, recycling, and management. *Waste Manag.* **2018**, *78*, 318–330. [CrossRef] [PubMed]
6. Ahmedzade, P.; Sengoz, B. Evaluation of steel slag coarse aggregate in hot mix asphalt concrete. *J. Hazard. Mater.* **2009**, *165*, 300–305. [CrossRef]
7. Liu, J.; Wang, Z.; Guo, H.; Yan, F. Thermal transfer characteristics of asphalt mixtures containing hot poured steel slag through microwave heating. *J. Clean. Prod.* **2021**, *308*, 127225. [CrossRef]
8. Asi, I.M. Evaluating skid resistance of different asphalt concrete mixes. *Build. Environ.* **2007**, *42*, 325–329. [CrossRef]
9. Wu, S.; Xue, Y.; Ye, Q.; Chen, Y. Utilization of steel slag as aggregates for stone mastic asphalt (SMA) mixtures. *Build. Environ.* **2007**, *42*, 2580–2585. [CrossRef]
10. Xue, Y.; Wu, S.; Hou, H.; Jin, Z. Experimental investigation of basic oxygen furnace slag used as aggregate in asphalt mixture. *J. Hazard. Mater.* **2006**, *138*, 261–268. [CrossRef]
11. Cui, P.; Wu, S.; Xiao, Y.; Hu, R.; Yang, T. Environmental performance and functional analysis of chip seals with recycled basic oxygen furnace slag as aggregate. *J. Hazard. Mater.* **2020**, *405*, 124441. [CrossRef]
12. Oluwasola, E.A.; Hainin, R.; Maniruzzaman, M.; Aziz, A. Evaluation of rutting potential and skid resistance of hot mix asphalt incorporating electric arc furnace steel slag and copper mine tailing. *Indian J. Eng. Mater. Sci.* **2015**, *22*, 550–558.
13. Liapisa, I.; Likoydisb, S. Use of electric arc furnace slag in thin, skid-resistant surfacing. *Procedia Soc. Behav. Sci.* **2011**, *48*, 907–918. [CrossRef]
14. Hainin, M.R.; Rusbintardjo, G.; Hameed, M.; Hassan, N.A.; Yusoff, N.M. Utilisation of Steel Slag as an Aggregate Replacement in Porous Asphalt Mixtures. *J. Teknol.* **2014**, *69*. [CrossRef]
15. Sorlini, S.; Sanzeni, A.; Rondi, L. Reuse of steel slag in bituminous paving mixtures. *J. Hazard. Mater.* **2012**, *209–210*, 84–91. [CrossRef]
16. Ziari, H.; Nowbakht, S.; Rezaei, S.; Mahboob, A. Laboratory Investigation of Fatigue Characteristics of Asphalt Mixtures with Steel Slag Aggregates. *Adv. Mater. Sci. Eng.* **2015**, *2015*, 623245. [CrossRef]

17. Kavussi, A.; Jalili, Q.M.; Hassani, A. Fatigue behavior analysis of asphalt mixes containing electric arc furnace (EAF) steel slag. *J. Rehabil. Civ. Eng.* **2015**, *3*, 74–86. [\[CrossRef\]](#)
18. Fwa, T.F.; Yoong, C.C.; Than, T.N.; See, S.L. Development of Environmentally Sustainable Pavement Mix. *Int. J. Pavement Res. Technol.* **2013**, *6*, 440–446. [\[CrossRef\]](#)
19. Wang, G.; Wang, Y.; Gao, Z. Use of steel slag as a granular material: Volume expansion prediction and usability criteria. *J. Hazard. Mater.* **2010**, *184*, 555–560. [\[CrossRef\]](#)
20. Thomson, M. Why is types hydrated lime special? In Proceedings of the International Building Lime Symposium, Orlando, FL, USA, 9–11 March 2005.
21. Oluwasola, E.A.; Hainin, R.; Maniruzzaman, M.; Aziz, A. Evaluation of asphalt mixtures incorporating electric arc furnace steel slag and copper mine tailings for road construction. *Transp. Geotech.* **2015**, *2*, 47–55. [\[CrossRef\]](#)
22. Hesami, S.; Ameri, M.; Goli, H.; Akbari, A. Laboratory investigation of moisture susceptibility of warm-mix asphalt mixtures containing steel slag aggregates. *Int. J. Pavement Eng.* **2015**, *16*, 745–759. [\[CrossRef\]](#)
23. Coomarasamy, A.; Walzak, T. Effects of moisture on surface chemistry of steel slags and steel slag-asphalt paving mixes. *Transp. Res. Rec.* **1995**, *1492*, 85–95.
24. Chen, Z.; Xie, J.; Xiao, Y.; Chen, J.; Wu, S. Characteristics of bonding behavior between basic oxygen furnace slag and asphalt binder. *Constr. Build. Mater.* **2014**, *64*, 60–66. [\[CrossRef\]](#)
25. Klonica, M.; Kuczmazewski, J. Determining the value of surface free energy on the basis of the contact angle. *Adv. Sci. Technol. Res. J.* **2017**, *11*, 66–74. [\[CrossRef\]](#)
26. Qazizadeh, M.J.; Farhad, H.; Kavussi, A.; Sadeghi, A. Evaluating the Fatigue Behavior of Asphalt Mixtures Containing Electric Arc Furnace and Basic Oxygen Furnace Slags Using Surface Free Energy Estimation. *J. Clean. Prod.* **2018**, *188*, 355–361. [\[CrossRef\]](#)
27. Zhang, J.; Apeagyei, A.K.; Airey, G.D.; Grenfell, J.R.A. Influence of aggregate mineralogical composition on water resistance of aggregate-bitumen adhesion. *Int. J. Adhes. Adhes.* **2015**, *62*, 45–54. [\[CrossRef\]](#)
28. Aguiar-Moya, J.P.; Baldi-Sevilla, A.; Salazar-Delgado, J.; Pacheco-Fallas, J.F.; Loria-Salazar, L.; Reyes-Lizcano, F.; Cely-Leal, N. Adhesive properties of asphalts and aggregates in tropical climates. *Int. J. Pavement Eng.* **2016**, *19*, 738–747. [\[CrossRef\]](#)
29. Chen, Z.; Wu, S.; Xiao, Y.; Zeng, W.; Yi, M.; Wan, J. Effect of hydration and silicone resin on Basic Oxygen Furnace slag and its asphalt mixture. *J. Clean. Prod.* **2016**, *112*, 392–400. [\[CrossRef\]](#)
30. Zhu, J.; Wu, S.; Zhong, J.; Wang, D. Investigation of asphalt mixture containing demolition waste obtained from earthquake-damaged buildings. *Constr. Build. Mater.* **2012**, *29*, 466–475. [\[CrossRef\]](#)
31. Aguiar-Moya, J.P.; Salazar-Delgado, J.; Baldi-Sevilla, A.; Leiva-Villacorta, F.; Loria-Salazar, L. Effect of Aging on Adhesion Properties of Asphalt Mixtures with the Use of Bitumen Bond Strength and Surface Energy Measurement Tests. *Transp. Res. Rec. J. Transp. Res. Board.* **2015**, *2505*, 57–65. [\[CrossRef\]](#)
32. Bhasin, A.; Masad, E.; Little, D.; Lytton, R. Limits on Adhesive Bond Energy for Improved Resistance of Hot-Mix Asphalt to Moisture Damage. *Transp. Res. Rec. J. Transp. Res. Board.* **2006**, *1970*, 3–13. [\[CrossRef\]](#)
33. Howson, J.; Masad, E.; Bhasin, A.; Little, D.; Lytton, R. Comprehensive analysis of surface free energy of asphalts and aggregates and the effects of changes in pH. *Constr. Build. Mater.* **2011**, *25*, 2554–2564. [\[CrossRef\]](#)
34. Guo, J.; Bao, Y.; Min, W. Study on the adhesion property between asphalt binder and aggregate: A state-of-the-art review. *Constr. Build. Mater.* **2020**, *256*, 119474. [\[CrossRef\]](#)
35. Skaf, M.; Manso, J.M.; Aragón, Á.; Fuente-Alonso, J.A.; Ortega-López, V. EAF slag in asphalt mixes: A brief review of its possible re-use. *Resour. Conserv. Recycl.* **2017**, *120*, 176–185. [\[CrossRef\]](#)
36. Su, Z.; Muhammad, Y.; Sahibzada, M.; Li, J.; Zhang, L. Preparation and properties of aminated graphene fiber incorporated modified asphalt. *Constr. Build. Mater.* **2019**, *229*, 116836. [\[CrossRef\]](#)
37. Guo, C.; Han, S.; Han, R. Evaluation of asphalt-aggregate adhesion using surface free energy theory. *Appl. Mech. Mater.* **2014**, *686*, 51–56. [\[CrossRef\]](#)
38. Shafabakhsh, G.H.; Faramarzi, M.; Sadeghnejad, M. Use of Surface Free Energy method to evaluate the moisture susceptibility of sulfur extended asphalts modified with antistripping agents. *Constr. Build. Mater.* **2015**, *98*, 456–464. [\[CrossRef\]](#)
39. Moraes, R.; Velasquez, R.; Bahia, H. Using bond strength and surface energy to estimate moisture resistance of asphalt-aggregate systems. *Constr. Build. Mater.* **2017**, *130*, 156–170. [\[CrossRef\]](#)
40. Pasetto, M.; Baldo, N. Influence of the aggregate skeleton design method on the permanent deformation resistance of stone mastic asphalt. *Mater. Res. Innov.* **2015**, *18*, S3-96–S3-101. [\[CrossRef\]](#)
41. Wu, S.; Xue, Y.; Ye, Q.; Chen, Y. Performance Evaluation of Asphalt Mixes Containing Steel Slag Aggregate as a Measure to Resist Studded Tire Wear. *J. Mater. Civ. Eng.* **2016**, *28*. [\[CrossRef\]](#)
42. Ameri, M.; Hesami, S.; Goli, H. Laboratory evaluation of warm mix asphalt mixtures containing electric arc furnace (EAF) steel slag. *Constr. Build. Mater.* **2013**, *49*, 611–617. [\[CrossRef\]](#)

Disclaimer/Publisher’s Note: The statements, opinions and data contained in all publications are solely those of the individual author(s) and contributor(s) and not of MDPI and/or the editor(s). MDPI and/or the editor(s) disclaim responsibility for any injury to people or property resulting from any ideas, methods, instructions or products referred to in the content.